Impaired microglia process dynamics post-stroke are specific to sites of secondary neurodegeneration

Kluge, Murielle G.; Kracht, Laura; Abdolhoseini, Mahmoud; Ong, Lin Kooi; Johnson, Sarah J.; Nilsson, Michael; Walker, Frederick R.

Published in:
Glia

DOI:
10.1002/glia.23201

Received: 26 February 2017 | Revised: 6 July 2017 | Accepted: 23 July 2017

DOI: 10.1002/glia.23201

GLIA
WILEY

RESEARCH ARTICLE

Impaired microglia process dynamics post-stroke are specific to sites of secondary neurodegeneration

Murielle G. Kluge[1,2] | Laura Kracht[3] | Mahmoud Abdolhoseini[4] | Lin Kooi Ong[1,2,5] | Sarah J. Johnson[4] | Michael Nilsson[1,2,5] | Frederick R. Walker[1,2,5]

[1]School of Biomedical Sciences and Pharmacy and the Priority Research Centre for Stroke and Brain Injury, University of Newcastle, Callaghan, New South Wales, Australia

[2]Hunter Medical Research Institute, Newcastle, New South Wales, Australia

[3]Department of Neuroscience, University of Groningen, University Medical Centre Groningen, The Netherlands

[4]School of Electrical Engineering and Computer Science, University of Newcastle, Callaghan, New South Wales, Australia

[5]NHMRC Centre of Research Excellence Stroke Rehabilitation and Brain Recovery, Heidelberg, Victoria, Australia

Correspondence
Frederick R. Walker, Medical Science Building 306, University Drive, Callaghan, NSW 2308, Australia.
Email: rohan.walker@newcastle.edu.au

Funding information
National Health and Medical Research Council (NHMRC) of Australia; Hunter Medical Research Institute; Faculty of Health and Medicine Pilot Grant; The University of Newcastle, Australia

Abstract

Stroke induces tissue death both at the site of infarction and at secondary sites connected to the primary infarction. This latter process has been referred to as secondary neurodegeneration (SND). Using predominantly fixed tissue analyses, microglia have been implicated in regulating the initial response at both damage sites post-stroke. In this study, we used acute slice based multiphoton imaging, to investigate microglia dynamic process movement in mice 14 days after a photothrombotic stroke. We evaluated the baseline motility and process responses to locally induced laser damage in both the peri-infarct (PI) territory and the ipsilateral thalamus, a major site of post-stroke SND. Our findings show that microglia process extension toward laser damage within the thalamus is lost, yet remains robustly intact within the PI territory. However, microglia at both sites displayed an activated morphology and elevated levels of commonly used activation markers (CD68, CD11b), indicating that the standardly used fixed tissue metrics of microglial "activity" are not necessarily predictive of microglia function. Analysis of the purinergic P_2Y_{12} receptor, a key regulator of microglia process extension, revealed an increased somal localization on nonresponsive microglia in the thalamus. To our knowledge, this is the first study to identify a nonresponsive microglia phenotype specific to areas of SND post-stroke, which cannot be identified by the classical assessment of microglia activation but rather the localization of P_2Y_{12} to the soma.

KEYWORDS
laser injury, live cell multiphoton imaging, P_2Y_{12} receptor, peri-infarct, thalamus

1 | INTRODUCTION

Stroke is defined as a disruption, usually of an occlusive thromboembolic nature, within the cerebrovascular network (Krishnamurthi et al., 2013). It is well recognized that stroke induces substantial death of tissue at and around the site of the occlusion (known as the infarct) but also leads to a second injury process, a phenomenon increasingly referred to as secondary neurodegeneration (SND) (Block, Dihne, & Loos, 2005; Dirnagl, Iadecola, & Moskowitz, 1999; Zhang, Zhang, Xing, Liang, & Zeng, 2012). SND involves the progressive death of neurons that were connected to the site of infarction but not initially damaged by the stroke. SND unfolds over a longer time scale than the infarction process and has recently been implicated as a potential modulator to a number of late phase functional recovery disturbances (Chen, Garcia, Huang, & Constantini, 2014; Dang et al., 2016; Fernandez-Andujar et al., 2014).

Microglia have a central role in responding to stroke-induced tissue damage within the peri-infarct (PI) territories and at sites of SND. Highlighting the importance of microglia, Lalancette-Hebert et al. and Szalay et al. have demonstrated that conditional removal of microglia exaggerates the severity of stroke-induced tissue loss (Lalancette-Hebert, Gowing, Simard, Weng, & Kriz, 2007; Szalay et al., 2016). The extent to which microglia exert neuroprotective functions at sites of SND is currently uncharacterized. However, Jones et al. and Ong et al. have both described an association between suppression of microglia responses with increased neuronal loss at sites of SND post-stroke (Jones et al., 2015).

Microglia are a very diverse and dynamic cell population, constantly moving their processes, migrating and changing their

morphology in order facilitate a variety of functions. However, most of what is known about microglia function has come from studies undertaken on fixed tissue and protein or RNA expression profiles. Activated microglia in the PI territories and sites of SND are often classified on snapshots of their morphology and the expression of classical microglia activation markers (e.g., CD11b, Iba-1, and CD68). However, these methods are useful for a general classification of microglia but do not assess microglia function directly.

To directly address the functional properties of microglia, it has become increasingly common to use in-vivo and ex-vivo imaging techniques to investigate microglia in real time as so many microglia functions are dependent on extensive structural remodeling (e.g,. directed process movement, somal migration) (Schafer, Lehrman, & Stevens, 2013; Sipe et al., 2016; Tremblay, Lowery, & Majewska, 2010). Process motility is considered an essential feature of normal microglia function within the healthy central nervous system (CNS) as well as being involved in the response to tissue insult, injury and disease (Fetler & Amigorena, 2005; Ohsawa & Kohsaka, 2011; Wake, Moorhouse, & Nabekura, 2011; Walker et al., 2014). Particularly critical is the ability of the cells to extend and retract their numerous fine processes to sites of interest within their microenvironment (Tremblay & Majewska, 2011). Commonly used assays to investigate microglia process dynamics are the measurement of baseline motility and directed process response towards a locally induced laser injury (Davalos et al., 2005; Dissing-Olesen et al., 2014; Haynes et al., 2006; Hines, Hines, Mulligan, & Macvicar, 2009; Nimmerjahn, Kirchhoff, & Helmchen, 2005; Sieger, Moritz, Ziegenhals, Prykhozhij, & Peri, 2012). Both assays are used to assess microglia responsiveness and their ability to sense and react to changes in their microenvironment.

One of the best characterized modulators of microglia process movement is the purinergic P_2Y_{12} receptor, mediating process extension towards tissue damage via binding of ATP (Davalos et al., 2005; Haynes et al., 2006; Honda et al., 2001; Ohsawa et al., 2010). P_2Y_{12} receptors are exclusively expressed on microglia within the brain and, under non-pathological settings, are predominantly located on distal ramified process tips (Sasaki et al., 2003; Sipe et al., 2016). P_2Y_{12} signaling is not only required for process extension toward sites of damage but seems to also be involved in microglia recruitment to other sites of interest such as neuronal dendrites and spines during synaptic plasticity (Eyo et al., 2015; Sipe et al., 2016; Tremblay et al., 2010; Wake, Moorhouse, Jinno, Kohsaka, & Nabekura, 2009).

In this study, we aimed to investigate the dynamic properties of microglia after stroke, focusing on classically activated microglia at both the primary infarction as well as microglia within thalamic areas of SND. We are using a photothrombotic occlusion model in transgenic Cx3CR1$^{GFP/WT}$ mice, expressing GFP-labeled microglia in combination with ex-vivo live cell multiphoton imaging or fixed and fresh frozen tissue analysis. To our knowledge, we are the first to investigate and link microglia process motility and live dynamics to morphological assessment and expression patterns, which are widely accepted to correlate with functional activity.

2 | MATERIALS AND METHODS

2.1 | Animals

All experiments were carried out in 6–8 week old male heterozygous Cx3CR1$^{GFP/WT}$ mice, obtained from Jackson Laboratories, expressing EGFP under the control of the endogenous Cx3CR1 (fractalkine receptor) promotor. This receptor is ubiquitously expressed by microglia in the brain as well as in monocytes, dendritic cells, and natural killer cells thorough the body. Experiments were approved by the University of Newcastle Animal Care and Ethics Committee, and conducted in accordance with the New South Wales Animals Research Act and the Australian Code of Practice for the use of animals for scientific purposes.

2.2 | Photothrombotic occlusion

Strokes, 2.2 mm lateral of bregma, within the somatosensory cortex were induced using the photothrombotic occlusions protocol as previously described (Ong, Zhao, Kluge, Walker, & Nilsson, 2016; Patience et al., 2015). All further experiments and tissue processing was performed on day 14 post-stroke.

2.3 | Morphological analysis

Morphological analysis was performed on confocal images taken from 30 μm fixed Cx3CR1$^{GFP/WT}$ brain sections. Cx3CR1$^{GFP/WT}$ whole brain images were taken and merged, using the LAX software and tile scanning mode with a Leica HC 10x objective, generating z-stack images encompassing the entire thickness of the section at a step size of 1.5 μm. Imaging for morphological analyses was performed on a Nikon Eclipse 90i microscope with a 20× lens (0.75 NA, Nikon) and NIS Elements software, respectively. Z-stack images of the entire 30 μm slice were taken with a step size of 1.5 μm. All confocal images were exported as maximum z-projection images for off line analysis.

Quantitative analysis of soma and branch parameters was performed using a combined multilevel thresholding and minimum spanning tree skeleton tracing approach as described in Abdolhoseini et al. (Figure 2a; Mahmoud Abdolhoseini & Johnson, 2016). A schematic illustration of the assessed parameters can be found in Supporting Information Fig. S2. Sham groups were used as the primary comparators and absolute values are presented in Supporting Information Table S2. See Supporting Information for more detail.

2.4 | Immunohistochemistry and quantification of process to soma immunoreactivity

For immunofluorescence labeling, free-floating, 30 μm PFA fixed sections were immunostained using standard protocols as previously described (Tynan et al., 2013). In-depth protocols and antibody concentrations can be found in the Supporting Information information. High-resolution confocal images of immunolabeled brain sections were taken on a Leica TCS SP8 confocal microscope with a Leica HC PLC APO 40×/1.30 and 63×/1.40 OIL objective. For each region of interest,

identified in fluorescent mode, 20 μm z-stacks with a step size of 1 μm were taken at magnifications of 2×.

Quantification of immuno-reactive material for process to soma ratio was performed using a custom MatLab script (Figure 5g,h). Briefly, GFP fluorescent intensity and multilevel thresholding was used to distinguish soma from process signal. The intensity for the fluorescent material for the immunoreactive signal was calculated by overlaying the second channel. This analysis was run for a single, in focus cell, per image. Results from multiple microglia cells from the same animal were averaged.

2.5 | Acute slice preparation

For acute slice preparation, animals were perfused with 12 ml of an ice cold solution containing (in mM): 236 sucrose, 11 D-glucose, 25 $NaHCO_3$, 2.5 KCl, 1 NaH_2PO_4, 5.3 $MgCL_2$, and 1 $CaCL_2$. Brains were extracted and sliced into 150 μm (phagocytosis assay) and 300 μm (acute imaging) thick coronal sections, using a vibratome (Leica VT 1200S). Cortical brain sections between bregma 1.18 to −0.10 mm and thalamic brain sections between bregma −1.0 to −2.2 mm where selected for further processing.

Slices were incubated for 45 min at room temperature (RT) in artificial cerebral spinal fluid (aCSF) containing (in mM): 120 sucrose, 11 D-glucose, 26 $NaHCO_3$, 2.5 KCl, 1 NaH_2PO_4, 1 $MgCL_2$, and 2.5 $CaCL_2$, prior to further procedures. Both solutions were constantly oxygenated with 95% O_2 and 5% CO_2, adjusted to pH 7.3 and an osmolarity of 300 ± 5 mOsmol/kg (Osmomat 3000basic, Gonotec). All acute slice procedures and imaging was performed at RT under constant perfusion of aCSF.

2.6 | Ex-vivo two-photon slice imaging

A multiphoton scanning microscope (MaiTai laser; Spectra Physics coupled to a Leica TCS SP8 MP microscope with a Leica HC 25×/0.95 water objective with the Leica LAS X core software) was used to image acute brain sections. PI and thalamic areas of microglia activation, contralateral (CL) and the corresponding sham areas were identified in fluorescent mode. Fluorescently labeled microglia were imaged at a depth of ~100 μm within the tissue slice with a zoom of 2×. Z-stacks were 30 μm thick with a step size of 2 μm, resulting in a scan time of 1 min per stack. Images for time-lapse imaging were taken continuously every 1 min. EGFP was excited at 950 nm and emission detected with the Leica Hyd RLD detector. Laser ablations were induced by zooming into the middle of the image (48×) of the central *z*-plane and increasing the laser power to 100% for the scanning time of 1 s. Continuous time-lapse imaging started 5 s after the induction of the ablation and lasted for 15 min. Z-projections for each time point were created and aligned in their x-y plane using the StackReg plugin in Fiji is just ImageJ (FIJI, 1997–2013; NIH; http://imagej.nih.gov/ij/). Quantification of the microglia process response to a laser ablation was measured as average pixel intensity (*I*) within a 10 μm radius around the laser ablation over time [Process response = $(I_t - I_{t=1})/I_{t=1}$; Figure 4b). Baseline motility was assessed by creating difference images between each consecutive time point (Fiji) and calculating the ratio of average pixel intensity (*I*) of the difference to original image ($M = I_{\text{difference } t=1 \text{ and } 2}/I_{t=1}$; Figure 3a). The average motility over 15 min was taken. The average pixel intensity for a specific area within or for an entire image sequence was calculated using a custom MatLab script.

2.7 | Phagocytosis assay and quantitative analysis

Analysis of phagocytic activity in cortical and thalamic areas after stroke was performed in acute coronal brain slices prior to fixation and confocal imaging. Carboxylated red fluorescent microspheres (Thermo Fisher Scientific) were coated in 1% fetal calf serum, washed and resuspended in aCSF. Brain slices were incubated with microspheres ($2.2*10^5$ microspheres/ml) for 1 hr at 35°C. Slices were then washed in aCSF, drop-fixed in 4% PFA (pH 7.4) for 2 hr, mounted and cover-slipped. Z-stacks of 30 μm thickness with a step size of 1 μm were taken using Leica HC 25×/0.95 water objective, beginning from the top of the slice. Z-projections of both color channels were analyzed using a custom MatLab script. The amount of bead pixels (red) and the amount of cell pixels (green), as well as bead pixels located inside soma pixels (red in green) were identified after Otsu's thresholding. A minimum bead size of 1.5 μm^2 for the red channel, and a minimum soma size of 30 μm^2 for the green channel were set to exclude background particles and cell fragments. Phagocytic activity was calculated as average number of phagocytosed bead pixels per cell for each image.

2.8 | Protein extraction and western blotting

Protein extraction and western blotting analysis against amyloid β, $P_2Y_{12}R$, CD11b, CD68, and Cx3CR1 were performed using standard protocols, as previously described. See Supporting Information (Ong et al., 2014, 2016).

2.9 | Statistics

Statistical comparisons between groups were made using Prism 6 for Windows Version 6.01 statistical analysis software (GraphPad, La Jolla, CA). All values reported are mean ± *SEM*. Data was analyzed using one-way (one parameter) or two-way analysis (comparing multiple parameters) of variance (ANOVA) followed by Turkey's and Sidak's post hoc comparison, respectively. $p < .05$ was considered statistically significant.

3 | RESULTS

3.1 | Microglia at the infarct site and within the thalamus show a classically activated morphology 14 days after stroke

Previous studies of microglia morphology post-stroke have shown microglia "activation," characterized by deramified cells with a generally amoeboid appearance. This phenotype was observed both in the PI area and in sites of SND, most notably within the thalamus, and has

been shown to persist for several months post-stroke (Jones et al., 2015; Ong et al., 2016; Zhang et al., 2012).

Mosaic imaging of entire brain section from Cx3CR1$^{GFP/WT}$ sham and stroke animals 14 days post-stroke revealed substantial macrolevel disturbances in the GFP signal within the PI and thalamic territories (Figure 1a). Morphological analysis was subsequently undertaken within these regions, the stroked (ipsilateral), and nonstroked hemispheres (CL) of the somatosensory cortex and thalamus (Figure 1b). Areas of morphologically disturbed microglia in the thalamus colocalized with a loss of mature neurons and were therefore considered sites of SND (Supporting Information Fig. S1).

Morphological analysis comparing differences between each brain region in the strokes animals to their respective sham regions indicated that the PI cortex and the ipsilateral (IL) thalamus had undergone a shift toward a classically activated phenotype (Figure 2b,c). Relative to the sham group, microglia within the PI cortex and the IL thalamus exhibited a significant increase in the number of GFP positive cells and an increase in mean cell solidity and cell extent. Additionally, the cells exhibited significant reductions in the number and the length of secondary branches, as well as a reduced mean cell area.

Microglia within both the PI and ipsilateral thalamus after stroke would be considered classically activated. However, the direct comparison between both areas indicated a variety of significant differences (Figure 2d). Most notably, there was marked increase in the number of microglia within the thalamus (~2 fold differences) as well as a statistically greater increase in cell solidity and cell extent. Secondly, the soma area of thalamic microglia was found to have significantly increased whereas the soma area of PI microglia remained unchanged. Lastly, we observed differences in the primary branching structures between the two sites. Specifically, thalamic microglia showed no reduction in the number of primary branches, whereas the number of primary branches in cortical microglia reduced significantly.

3.2 | Microglia process extension toward sites of laser damage is reduced within the thalamus after stroke

Microglia responsiveness for all regions of interest was evaluated using acute slice preparation followed by multiphoton imaging. This approach allowed the visualization of activated microglia located deep within the thalamic region of the brain, a region that cannot be visualized using in-vivo imaging techniques of cortical structures. We evaluated both non-directed baseline motility and the directed process extension in response to laser damage. Baseline motility was quantified as motility index over 15 min by generating difference images obtained for a 15 min time sequence, and calculating the number of pixels that differ between two consecutive time points (Figure 3a). This approach evaluates all changes in cellular movement, process retraction, and extension. The motility index was obtained by calculating the average ratio between the difference and the original images over 15 min, one image per min. Our analysis indicated that microglia processes were motile in all regions in both stroked and sham animals (Figure 3b and Supporting Information movie S1–S4). However, we did observe modest reductions in process motility within the PI cortex and IL thalamus of stroked animals.

Directed process extension was evaluated in response to a laser damage for all regions of interest (Figure 4a). This procedure involves the exposure of tissue to a controlled high-intensity laser light, which induces rapid death of the targeted tissue. In response, microglia have consistently been shown to extend their processes towards the site of damage (Davalos et al., 2005; Haynes et al., 2006). The microglia process response was measured as an increase of average pixel intensity (I) within a 10 μm radius around the laser ablation over time, representing the increase of fluorescent material to that area (Figure 4b).

Microglia in all cortical areas (both stroke and sham) responded to the laser damage in a robust and consistent fashion, by extending their processes towards the site of damage (Supporting Information movie S5 and S6). Cells within a 30 μm radius of the ablation began to respond, on average, within 5 min of post-ablation and all processes reached the site of damage after 15 min, thereby increasing the amount of fluorescent material in the 10 μm analysis zone (Figure 4c,e).

In contrast to the PI, cells within the thalamus after stroke failed to respond to the laser damage (Figure 4d,f and Supporting Information movie S7 and S8). The microglia response within the CL thalamus of stroked animals after 15 min was strongly reduced and nearly totally absent for microglia in the IL thalamus, compared with the response in sham animals (Figure 4g). A similar loss of microglia dynamic function has been previously described in Alzheimer's pathology associated with close proximity to Aβ plaques (Gyoneva, Swanger, Zhang, Weinshenker, & Traynelis, 2016; Krabbe et al., 2013). We therefore investigated a potential role of Aβ post-stroke. As soluble Aβ oligomers were increased in both the PI and thalamic regions post-stroke, Aβ seems unlikely to represent a significant factor in reducing microglia responses towards laser damage in areas of SND (Supporting Information Fig. S3).

3.3 | Altered thalamic P_2Y_{12} protein expression and distribution

To further address the question as to why microglia fail to extend their processes towards locally introduced damage in areas of SND, we investigated the involvement of the main chemoattractant signaling pathway involved in process extension (Haynes et al., 2006; Orr, Orr, Li, Gross, & Traynelis, 2009).

We assessed P_2Y_{12} receptor protein levels for cortical and thalamic regions 14 days after occlusion compared with sham areas (Figure 5a). The P_2Y_{12} receptor was down-regulated in the infarct area but not significantly changed within the thalamus after stroke when compared with sham animals.

Immunofluorescent analysis of P_2Y_{12} additionally revealed a change in the distribution of the receptor on the microglia cell surface of activated microglia in the thalamus (Figure 5b,c). Fluorescent blots across the microglia cell soma clearly indicated increased amounts of P_2Y_{12} fluorescent material on the soma area of microglia in the IL thalamus after stroke (Figure 5d,e). Quantification, by calculating the process to soma ratio of the P_2Y_{12} specific fluorescent material, showed a

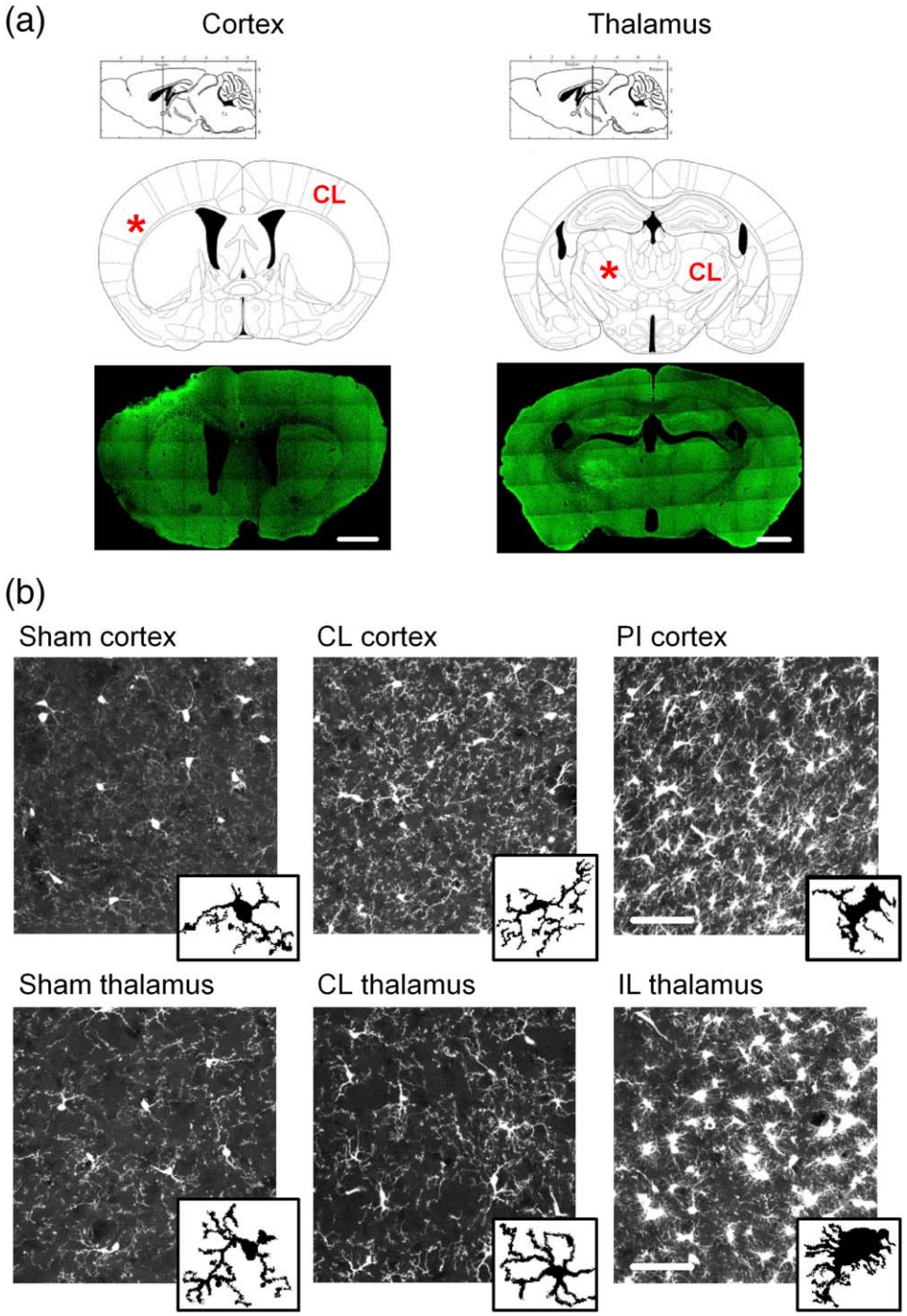

FIGURE 1 Microglia morphology at the PI and sites of SND 14 days after photothrombotic occlusion. (a) Schematic pictures (upper panel) adapted from "Paxinos & Franklin (2001). The Mouse Brain in Stereotaxic Coordinates. Elsevier" and representative confocal tile-scans images for whole Cx3CR1$^{WT/GFP}$ brain slices (lower panel) illustrating the two major regions of interest, the infarct site of the cortex and site of SND within the ipsilateral thalamus 14 days after photothrombotic occlusion. Fluorescently labeled microglia are green and areas of high microglia disturbance at the infarct site and within the ipsilateral thalamus are visible as brighter green regions in the confocal images (lower panel). High magnification confocal images for morphological microglia analysis were taken from the damaged hemispheres PI area (*) of the somatosensory and motor cortex at bregma 0.02 mm and thalamic regions (*) at bregma −1.82 mm. Confocal images were also taken in the corresponding CL regions and from sham animals without stroke. Scale bars, 1 mm. Grayscale LUT images can be found in Supporting Information fig. S5A. (b) Representative 30 μm z-stack confocal images of Cx3CR1$^{WT/GFP}$ mice 14 days after photothrombotic occlusion. Images were taken from the PI, CL, and sham regions of the cortex and the IL, CL, and sham areas of the thalamus as indicated in (a). Scale bars, 50 μm. Small inlay images illustrate a representative single cell remodeling using MicroTrac software [Color figure can be viewed at wileyonlinelibrary.com]

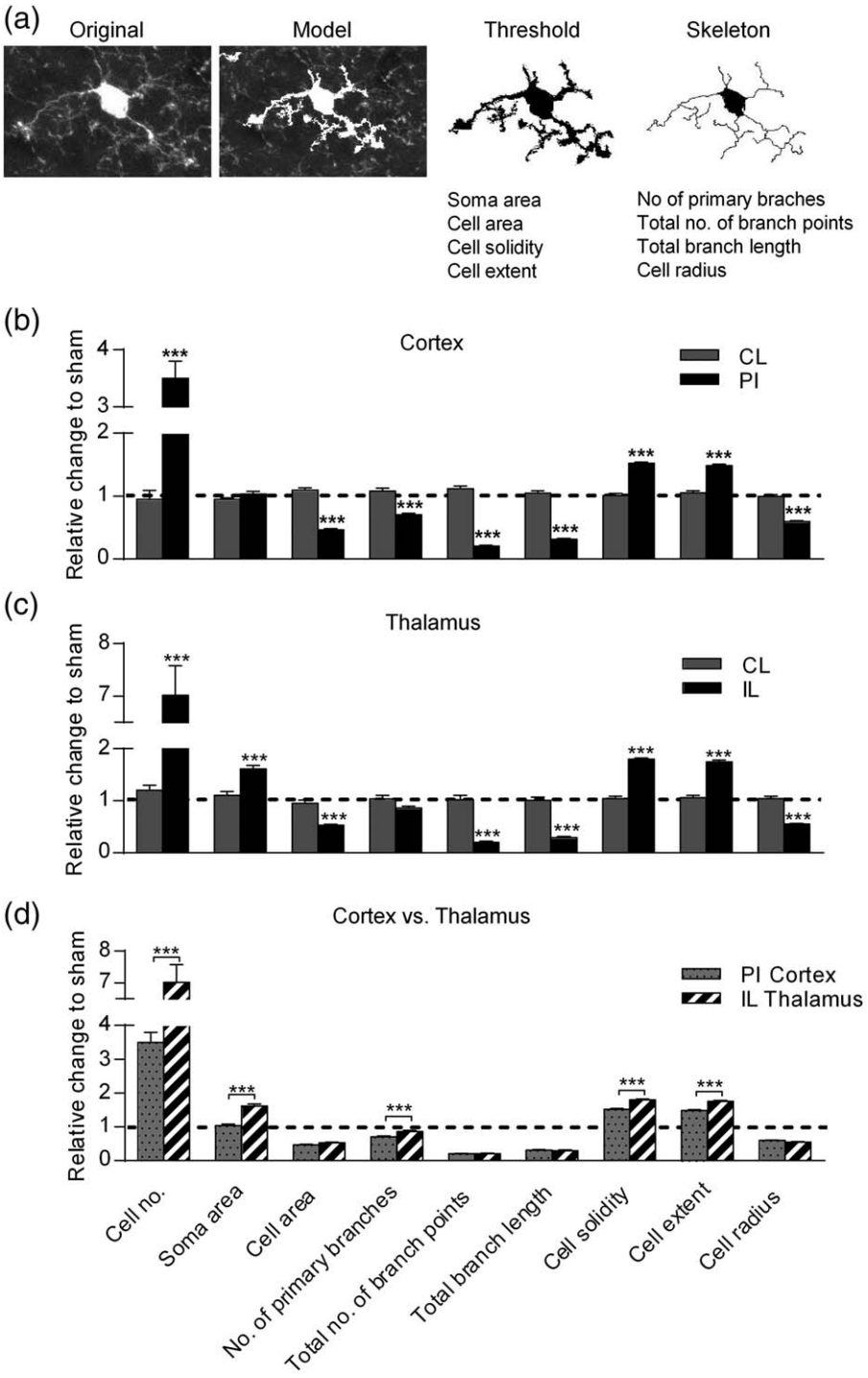

FIGURE 2 Morphological analysis of microglia cells shows remodeling towards an "activated" phenotype within the PI and the ipsilateral thalamus. (a) Illustrates the process of digital modeling based on the MicroTrac analysis platform. This process generated the formation of thresholded and skeletonized images, which were then used for morphological analysis. MicroTrac reconstruction was performed using multilevel thresholding combined with minimum spanning tree skeleton tracing (Mahmoud Abdolhoseini & Johnson, 2016). Soma area, as well as cell area, solidity, extent and cell radius were calculated using thresholding whereas the number of primary branches and branch points and length were evaluated by using the minimum spanning tree model. For more information, see Supporting Information. **(b and c)** Quantification of microglia morphology in cortical areas and thalamic regions, respectively, 14 days after photothrombotic occlusion. Confocal images from PFA fixed Cx3CR1$^{GFP/WT}$ brain slices of the corresponding areas after stroke and from sham animals were taken. Cells were reconstructed and analyzed in regard to morphologically relevant parameters [as indicated in (a)]. Parameters for each cell in the PI and CL area of the cortex and the IL and CL area of the thalamus after stroke were normalized to the mean of the sham area and expressed as mean ± *SEM* ($n = 5$ for sham and $n = 4$ for stroke animals). ***$p < .001$ (one-way ANOVA followed by Tukey's multiple comparisons). **(d)** A comparison of morphological parameters for microglia cells within the PI region of the cortex and the IL thalamus after stroke shown in b and c. ***$p < .001$ (two-way ANOVA followed by Sidak's multiple comparisons)

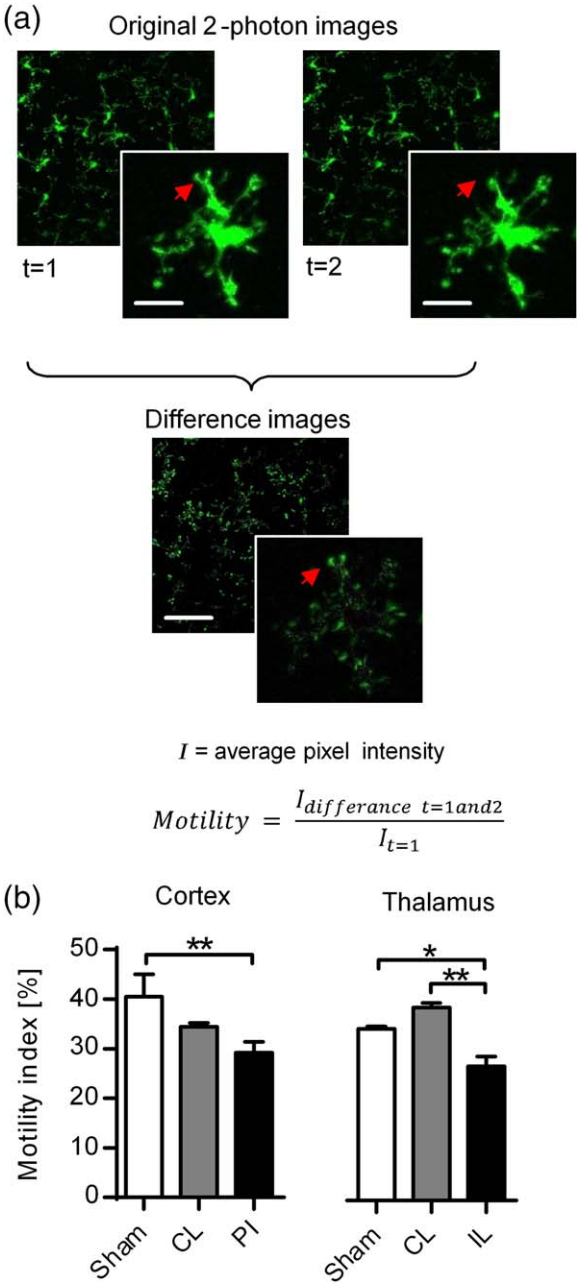

FIGURE 3 Microglia at both sites of damage are motile and viable, extending and retracting their processes. (a) Schematic showing the analysis of time-lapse images for microglia baseline motility. Difference images between two consecutive time points over 15 min are generated, displaying all pixels that are different between the two images, reflecting process extension and retraction. All images are processed without thresholding and the average pixel intensity for the original and difference images are calculated. Scale bare, 50 μm. Grayscale LUT images can be found in Supporting Information fig. S5. (b) Quantification of microglia baseline motility in cortical and thalamic areas 14 days after stroke and in sham operated animals. ($n = 4$, sham cortex; $n = 3$, CL cortex, $n = 8$, PI cortex; $n = 6$, sham thalamus; $n = 3$, CL thalamus; $n = 9$, IL thalamus). $^{*}p < .05$, $^{**}p < .01$, (one-way ANOVA followed by Tukey's multiple comparisons) [Color figure can be viewed at wileyonlinelibrary.com]

significantly reduced process to soma ratio for microglia in the IL thalamus compared with sham animals and the CL hemisphere (Figure 5g). Processes to soma ratios were unchanged in the PI regions after stroke (Figure 5f).

To validate a potential involvement the P_2Y_{12} mediated pathway in the reduced process response in the thalamus post-stroke, we measured microglia response to locally applied ATP. As a control, we introduced a pipette containing no ATP, ejecting only ACSF, observing no microglial response (Figure 6b). The application of 5 mM ATP, to thalamic sections of sham animals resulted in a robust microglial response involving process extension and process engulfment of the pipette tip (Figure 6a,b). In contrast, no process extension towards the pipette tip was visible within the ipsilateral thalamus after stroke.

To expand our understanding of differences between damage responsive and nonresponsive cells, we additionally characterized the expression of CD11b (a complement receptor), CD68 (up-regulated during phagocytosis) and Cx3CR1 (involved in neuron-microglia communication). Western blotting analysis indicated that CD11b and CD68 were increased at both sites of damage compared with sham animals (Figures 7a,b and 8a,b) while no differences were observed for Cx3CR1 (Supporting Information Fig. 4). Increases of CD68 and CD11b were additionally confirmed via immunofluorescent imaging (Figures 7c,d and 8c,d).

3.4 | Reduced phagocytic activity in the PI region but not the thalamus 14 days after stroke

To investigate whether other microglia functions might differ between the thalamus and the PI area after stroke, we assessed the phagocytic properties of microglia in acute brain slices using fluorescent microbeads (Figure 9a). As application of the beads to the brain slice resulted in a fragmentation of the round fluorescent beads, we calculated phagocytic activity as internalized pixels per cell, rather than beads per cell. Phagocytosis was reduced in the PI cortex when compared with sham slices, whereas no change in phagocytic activity was detected within the IL thalamus compared with the CL hemisphere or slices taken from sham animals (Figure 9b).

4 | DISCUSSION

Our study investigating microglia live process dynamics post-stroke lead to a series of interesting findings. Firstly, we describe a loss of microglia process extension toward the site of laser damage, which appears to be limited to areas of SND, as microglia within the PI region remain responsive to damage. Secondly, we show that the difference in microglia process response between both damage sites does not correlate with the assessment of morphological activation or the expression of the classical activation markers CD11b and CD68. Lastly, we investigated the involvement of the P_2Y_{12} receptor and found that non-responsive microglia in the thalamus displayed a strong localization of the receptor to the microglia soma.

Initial structural remodeling using fixed tissue slices indicated that microglia at both, the PI and the thalamus, had responded to the stroke

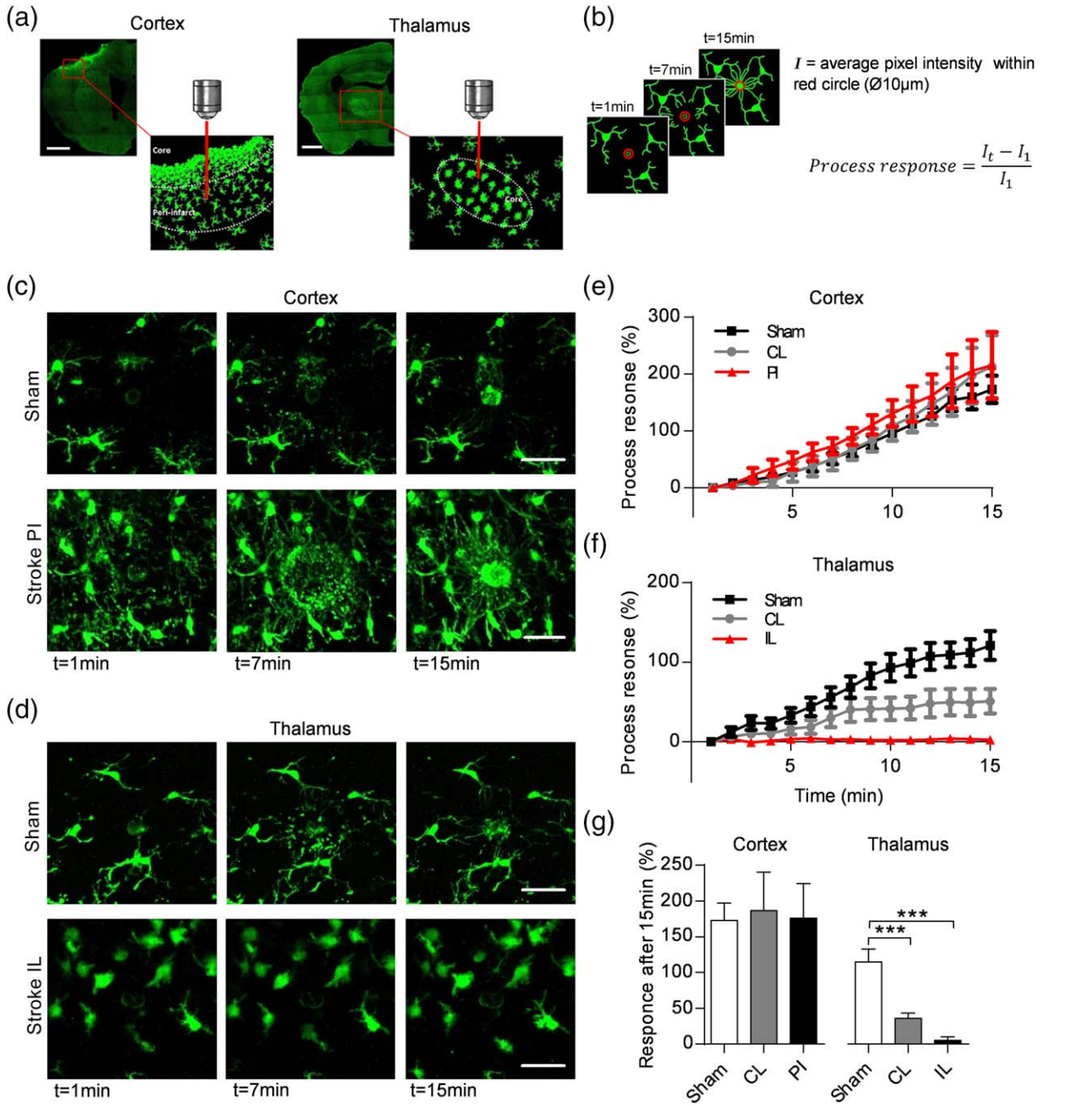

FIGURE 4 Acute sliced based multiphoton imaging reveals a strongly reduced microglia process response toward laser damage in the IL and CL thalamus. (a) Tile scan images and schematic cartoon indicating areas of microglia activation and positioning of the laser ablation during imaging of microglia motility. Laser ablations in the cortex were performed in the PI region, between the dotted line, whereas laser ablations in the thalamus were placed directly in the core of the IL activation outlined by the dotted circle. CL laser ablations were performed on the corresponding area on the CL hemisphere. (b) Schematic illustration and formula used to calculate process responses after laser ablation. Changes in fluorescent material F are calculated as average pixel intensity over time for a 10 μm Ø (red) around the center of the ablation. (c) Acute slice based two-photon imaging showing the microglia response following a laser injury. Microglia response within the cortex of a sham animal (upper panel) and the PI region 14 days after stroke (lower panel). Time points 1, 7, and 15 min after the induction of the laser ablation, visible as small focal auto-fluorescent circle, are shown. Scale bars, 30 μm. (d) Acute slice based two-photon imaging showing the microglia response following a laser injury. Microglia response within the thalamus of a sham animal (upper panel) and the ipsilateral (IL) thalamus 14 days after stroke (lower panel). Time points 1, 7, and 15 min after the induction of the ablation, visible as small focal autofluorescent circle, are shown. Scale bars, 30 μm. Grayscale LUT images can be found in Supporting Information fig. 5C. (e and f) Quantification of microglia responses over time for cortical areas (e) and thalamic areas (f). [$n = 18(8)$, sham cortex; $n = 11(6)$ PI cortex; $n = 6$ (3) CL cortex; $n = 13$ (7), sham thalamus; $n = 21(7)$ IL thalamus; $n = 12(6)$, CL thalamus; $n =$ ablation (animals)]. (g) Quantification of microglia response 15 min after the induction of the ablation shown in (e) and (f) $^{***}p < .001$ (one-way ANOVA followed by Tukey's multiple comparisons) [Color figure can be viewed at wileyonlinelibrary.com]

event by adopting a classically "activated" morphology of deramified branch structures (Figure 1). We therefore used ex-vivo imaging of acute brain slices, to image the dynamic properties of these activated microglia at both sites of classical "activation."

The baseline motility assay was done to characterize and understand the baseline process movement, associated with putative surveillance function as well as cell viability. Our analysis indicated that microglia within both the PI and thalamic sites post-stroke remain active in regards to their nondirected process movement. Overall, their motility was modestly reduced (27 and 21%, respectively) but might be due to the observed deramification of activated microglia (Figure 3 and Supporting Information movie S1–S4). The purpose of the process

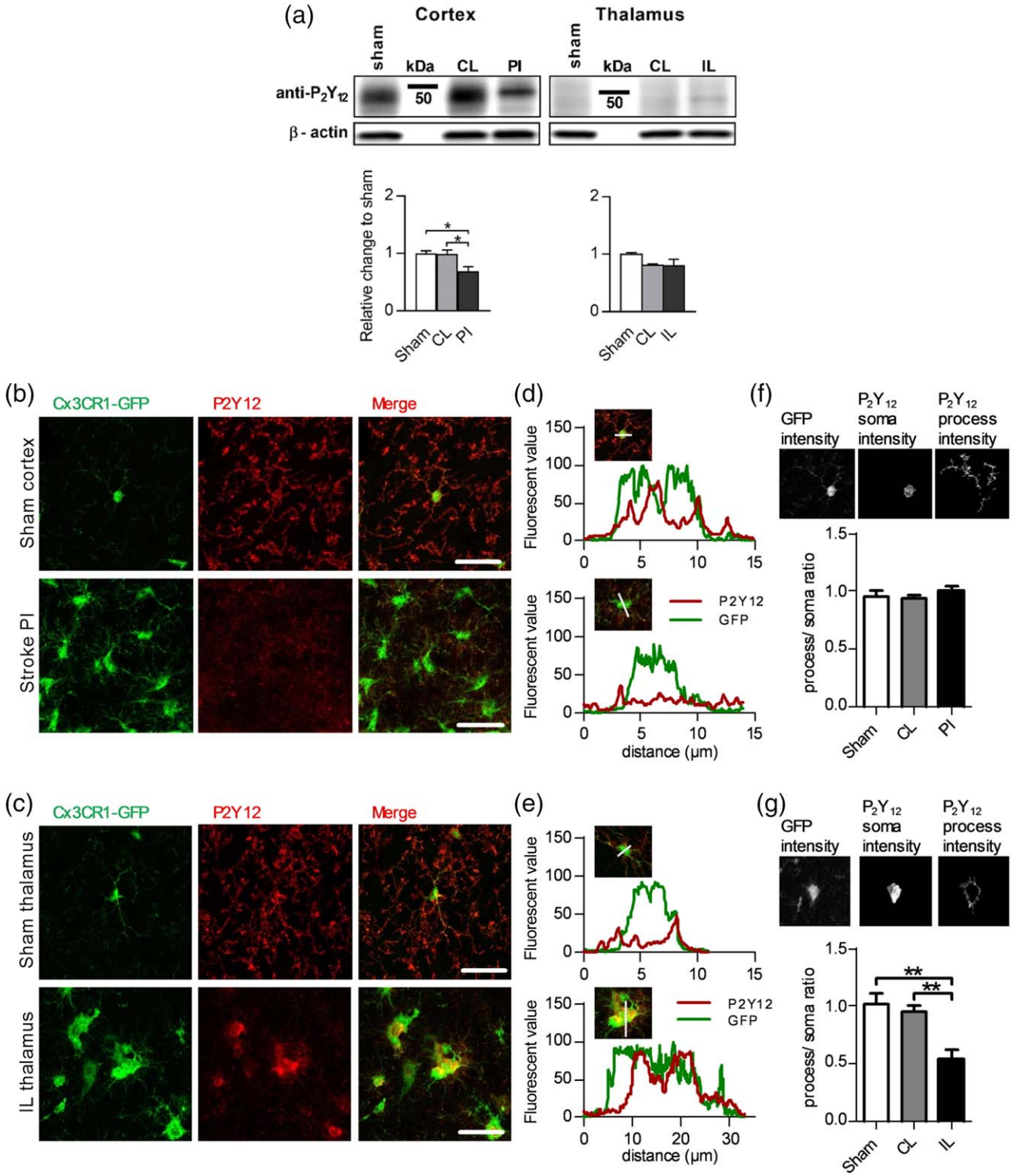

FIGURE 5.

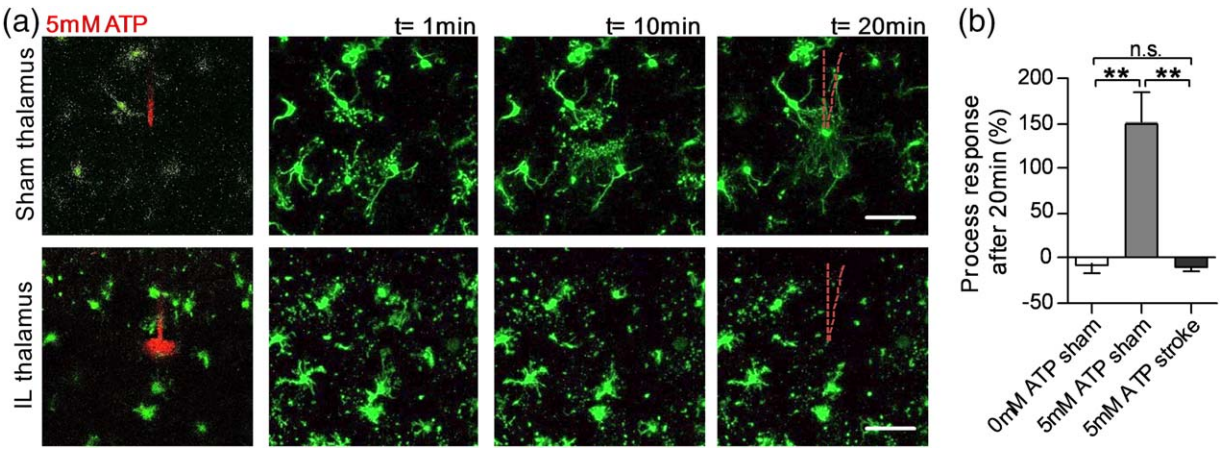

FIGURE 6 Microglia in the ipsilateral thalamus post-stroke show a strongly reduced response to local ATP application. (a) Acute slice based confocal (left panel) and two-photon imaging showing the microglia response following local application of 5 mM ATP. Confocal images (left panels) indicate the location of the pipette tip (red) during 100 ms puff application to the thalamic brain section. Two-photon images at time points 1, 10, and 20 min after ATP application are shown for thalamic sections of sham animals (top) and animals 14 days post-stroke (bottom). Scale bars, 30 μm. Grayscale LUT images can be found in Supporting Information Fig. S5E. (b) Quantification of microglia response 20 min after application of 0 or 5 mM ATP to thalamic brain sections ($n = 3$ applications per animal; $n = 3$ animals per group). $^{*}p < .05$, $^{**}p < .01$, $^{***}p < .001$ (one-way ANOVA followed by Tukey's multiple comparisons) [Color figure can be viewed at wileyonlinelibrary.com]

extension to laser damage assay was to characterize microglia ability to rapidly detect and approach sites of injury within the CNS, which is widely considered an essential microglia function (Davalos et al., 2005; Haynes et al., 2006). We found that this microglia response to local laser injury however was markedly different across both regions. Within the thalamus, process extension was significantly reduced within the CL thalamus and nearly totally abolished in the ipsilateral thalamus of stroked animals, whilst remaining robust within the PI territory post-stroke (Figure 4 and Supporting Information movie S5–S8). Additionally, the assessment of phagocytic function, evaluated as uptake of fluorescent material, also revealed differences across regions post-stroke. In particular, the phagocytic activity of microglia was reduced within the PI territories but remained unchanged in the thalamus when compared with sham animals (Figure 9).

These differences in live process movement and phagocytic function across regions are intriguing, in particular as both sites exhibit evidence of classical microgliosis. We show that microglia at both sites display very similar "activation" phenotypes when assessed using classical approaches such as morphological analysis, as well as increases in the microglia markers CD11b and CD68, the latter being a marker typically indicating phagocytic function (Figures 2–5b, 7, and 8) (Orr et al., 2009).

Taken together, these results clearly establish that the classical changes in morphology and increased expression of proteins such as CD11b and CD68 associated with functional activation are not absolute predictors of microglia dynamic behavior and function, particularly their responsiveness to laser injury.

The clear differences in microglia dynamic response within PI region and thalamus post-stroke led us to closely examine the morphological data obtained from the two sites using automated digital reconstruction. A comparative analysis indicated subtle differences, which can be summarized as a more pronounced "activation" phenotype of thalamic microglia. More specifically, a significantly larger soma area and a greater number of primary branches compared with microglia in the PI territory (Figure 2d). In a classical interpretation of morphological alteration, these subtle differences may be considered not particularly

FIGURE 5 P_2Y_{12} protein levels and distribution are different across activated microglia of the PI region and IL thalamus. (a) Representative western blot and quantification using anti-P_2Y_{12} antibody. Protein samples were taken 14 days post-stroke from the ipsi-and CL cortex and thalamus, compared with sham samples. Bands at molecular weights of 40 kD were analyzed. Data for all groups were expressed as a ratio of the mean ± *SEM* for each group relative to the mean of the sham group ($n = 5$ for sham and $n = 7$ for stroke groups). $^{*}p < .05$, $^{**}p < .01$, $^{***}p < .001$ (one-way ANOVA followed by Tukey's multiple comparisons). (b and c) Representative maximum projection, z-stack confocal images of cortical areas within the PI region (b) and ipsilateral thalamus (c) 14 days after occlusion (bottom panel) and within the corresponding areas of sham animals (top panels). Fixed brain slices of $Cx3CR1^{GFP/WT}$ mice expressing GFP- label microglia (left panel) were colabeled with anti-P_2Y_{12} antibody (middle panel). Merge in right panel (P_2Y_{12}: red; GFP: green). Scale bar, 25 μm. Grayscale LUT images can be found in Supporting Information Fig. S5D. (d and e) Representative fluorescent blots (P_2Y_{12}: red; GFP: green) for a cross section of a single microglia soma within the cortex (d), thalamus (e) of stroked animals (bottom panels, respectively) and corresponding sham animals (top panels). Inlay indicates the location of profile line across the cell. (f and g) Quantification of P_2Y_{12} process to soma immunoreactivity ratio for cortical (f) and thalamic regions (g) after stroke and in sham animals, respectively. Multilevel thresholding of the GFP fluorescent intensity was used to distinguish soma from process areas (left panels). The second channel for P_2Y_{12} immuno-reactive signal was then overlaid and the intensity for each region, soma (middle panel) and processes (right panel), was assessed. ($n = 3$ images per animal; $n = 4$ animals per group). $^{*}p < 0.05$, $^{**}p < 0.01$, $^{***}p < 0.001$ (one-way ANOVA followed by Tukey's multiple comparisons) [Color figure can be viewed at wileyonlinelibrary.com]

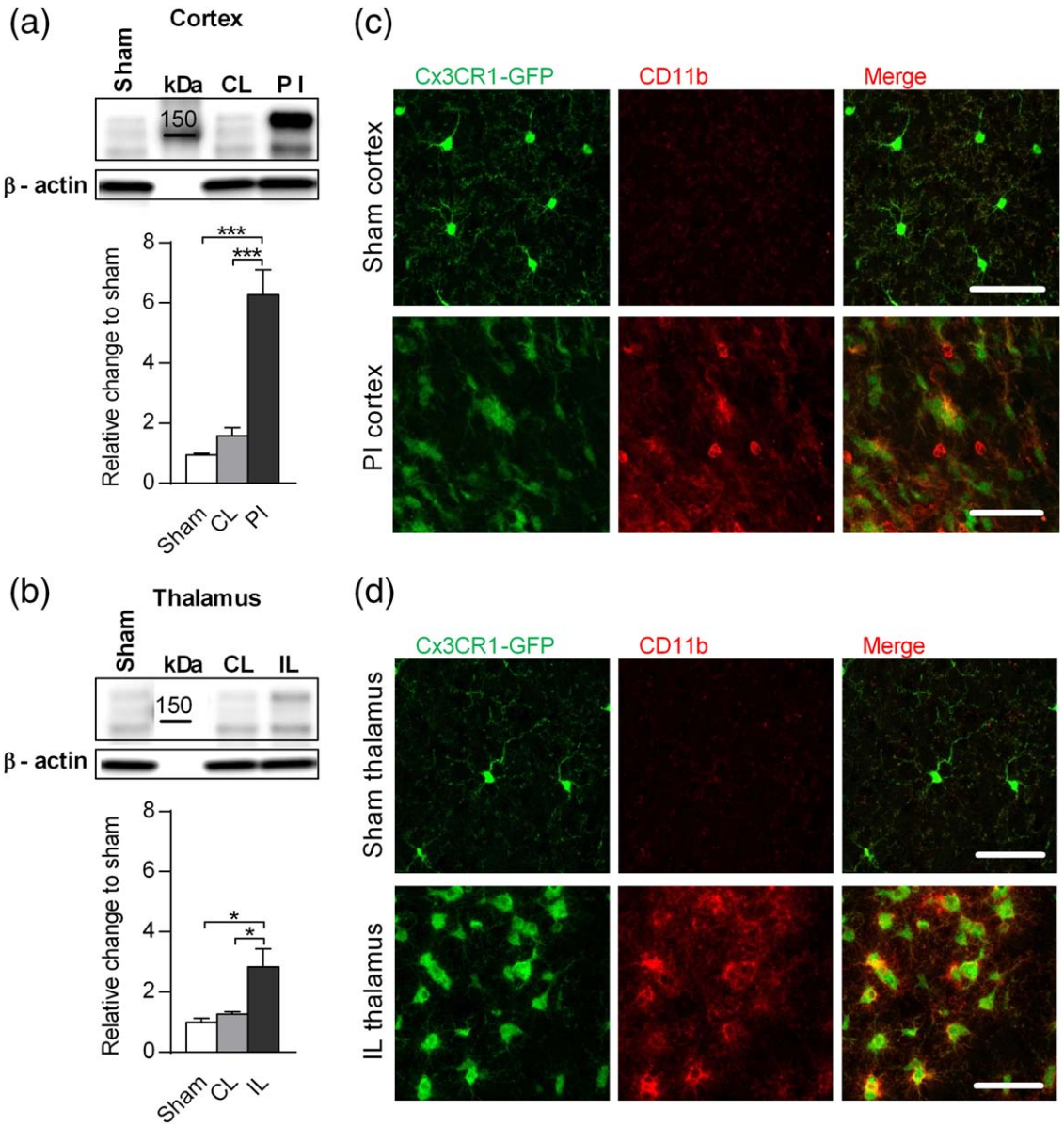

FIGURE 7 Increased expression of CD11b in both the PI territories and ipsilateral thalamus after stroke. (a and b) Representative western blot and quantification using anti-CD11b antibody of cortical (a) and thalamic regions (b). Protein samples were taken 14 days after PT stroke from the ipsi-and CL cortex and thalamus, compared with sham samples from animals without stroke. Bands at molecular weights of 160 kDa were analyzed. Data for all groups were expressed as a ratio of the mean ± *SEM* for each group relative to the mean of the sham group. [$n = 5$ for sham and (a) $n = 7$ (b) $n = 6$, and (c) $n = 8$ for stroke groups]. $^{*}p < .05$, $^{**}p < .01$, $^{***}p < .001$ (one-way ANOVA followed by Tukey's multiple comparisons). (c and d) Representative confocal images of cortical areas (c) and the thalamus (d) 14 days after occlusion (bottom panel) and within the corresponding areas of sham animals (top panels). Fixed brain slices of Cx3CR1 WT/GFP mice expressing GFP-label microglia (left panel) were colabeled with anti CD11b antibody (middle panel). Merge in right panel (CD11b:red; GFP:green). Scale bar, 25 μm. Grayscale LUT images can be found in Supporting Information Fig. S6A [Color figure can be viewed at wileyonlinelibrary.com]

relevant. However, in light of the apparent differences in microglia dynamic behavior, the here described differences may be connected to the nonresponsiveness of thalamic microglia.

The primary infarct and the secondary neurodegenerative injury are connected through the cortico-thalamic system, a circuit of neuronal projections connecting the primary motor and somatosensory cortex to multiple thalamic nuclei and back (Deschenes, Veinante, & Zhang, 1998; Hooks et al., 2013). After an infarction in the primary somatosensory cortex we observe neuronal loss and changes in microglial morphology consistent with a "classically activated" phenotype, most prominently within the ventral posteromedial nucleus (VPM) and the posterior complex of the thalamus (Supporting Information Fig. 1 and Figure 1a). The VPM, in particular, is implicated with the retrograde degeneration of sensory relay neurons after a cortical injury (Paz, Christian, Parada, Prince, & Huguenard, 2010). No changes in neuronal density or microglia morphology were observed in the CL thalamus; however, microglia within the VPM in the CL hemisphere showed a reduction in process response to laser damage (Figure 4f,g).

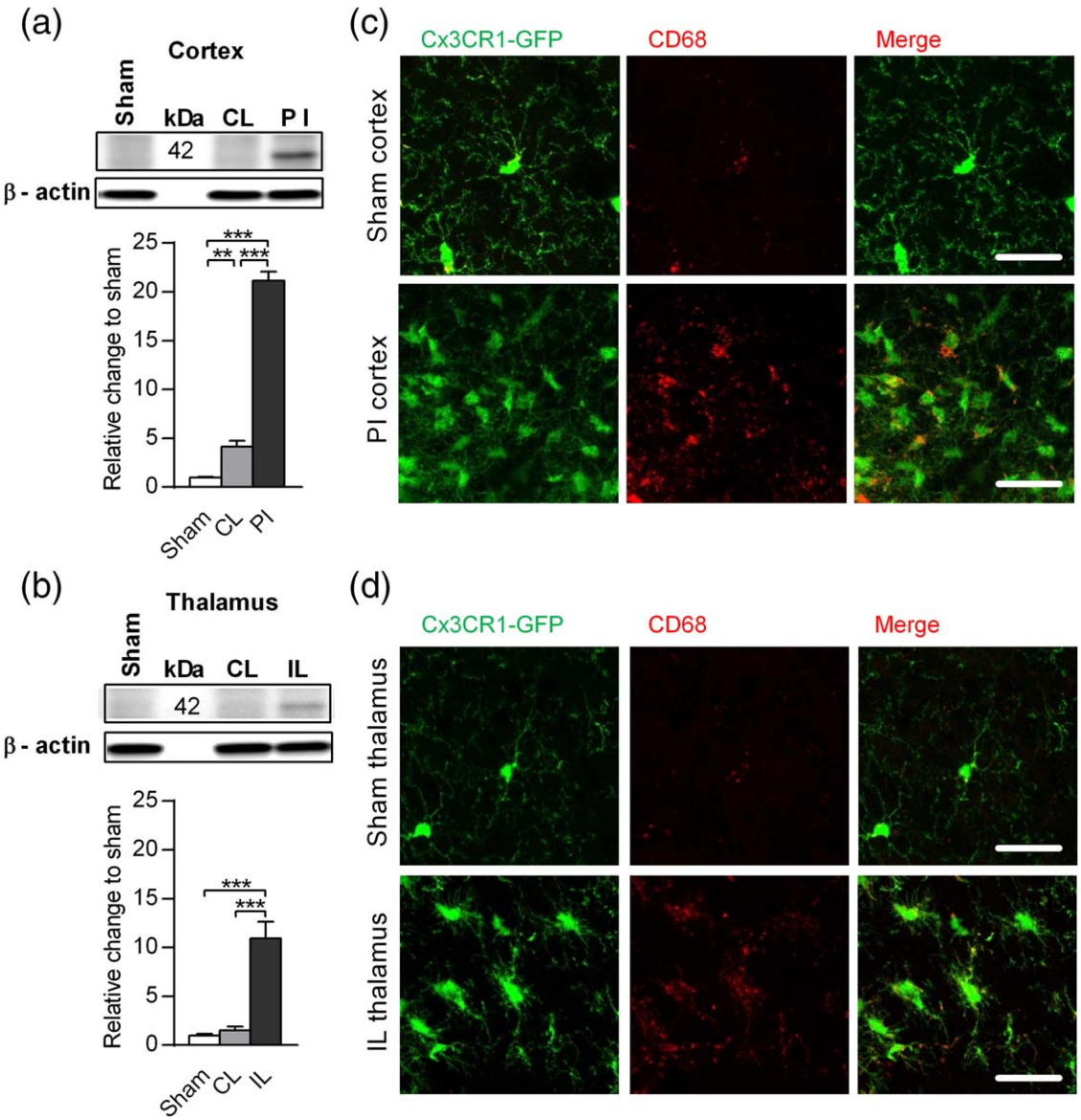

FIGURE 8 Increased expression of CD68 in both the PI territories and ipsilateral thalamus after stroke. (a and b) Representative western blot and quantification of CD68 protein in cortical (a) and thalamic (b) regions. Protein samples were taken 14 days after PT stroke from the ipsi-and CL cortex and thalamus, compared with sham samples from animals without stroke. Bands at molecular weights of 42 kDa were analyzed. Data for all groups were expressed as a ratio of the mean ± *SEM* for each group relative to the mean of the sham group. ($n = 5$ for sham and $n = 6$ for stroke groups). $^{*}p < .05$, $^{**}p < .01$, $^{***}p < .001$ (one-way ANOVA followed by Tukey's multiple comparisons). (c and d) Representative confocal images of cortical areas (c) and the thalamus (d) 14 days after occlusion (bottom panel) and within the corresponding areas of sham animals (top panels). Fixed brain slices of $Cx3CR1^{GFP/WT}$ mice expressing GFP- label microglia (left panel) were colabeled with anti CD68 antibody (middle panel). Merge in right panel (CD68:red; GFP:green). Scale bar, 25 μm. Grayscale LUT images can be found in Supporting Information Fig. S6B [Color figure can be viewed at wileyonlinelibrary.com]

Cross-hemispheric neuronal connections linking the thalamus might be contributing to this impaired microglia function in the CL thalamus (Mathiasen, Dillingham, Kinnavane, Powell, & Aggleton, 2017).

To our knowledge, we are the first to describe this loss of process response to a local laser damage in areas of SND post-stroke. However, impaired microglia process dynamics have been previously described in mouse models of Alzheimer's and Parkinson's pathologies. Microglia responses to a local injury were either significantly reduced or absent in two different mouse models of Alzheimer's disease, which was contributed to the close proximity of Aβ plaques (Gyoneva et al., 2016; Krabbe et al., 2013). Our data does not support a role for amyloid in driving the impaired migratory response of microglia within the thalamus, as the soluble Aβ oligomer load was also high at the PI area, where microglia responded robustly to the laser damage (Supporting Information Fig. 2). While there is evidence that Aβ plaques are present in the chronic phases after stroke, in our model 14 days after the infraction, there is no evidence of plaques within the brain (Ong et al., 2016; van Groen, Puurunen, Maki, Sivenius, & Jolkkonen, 2005). We

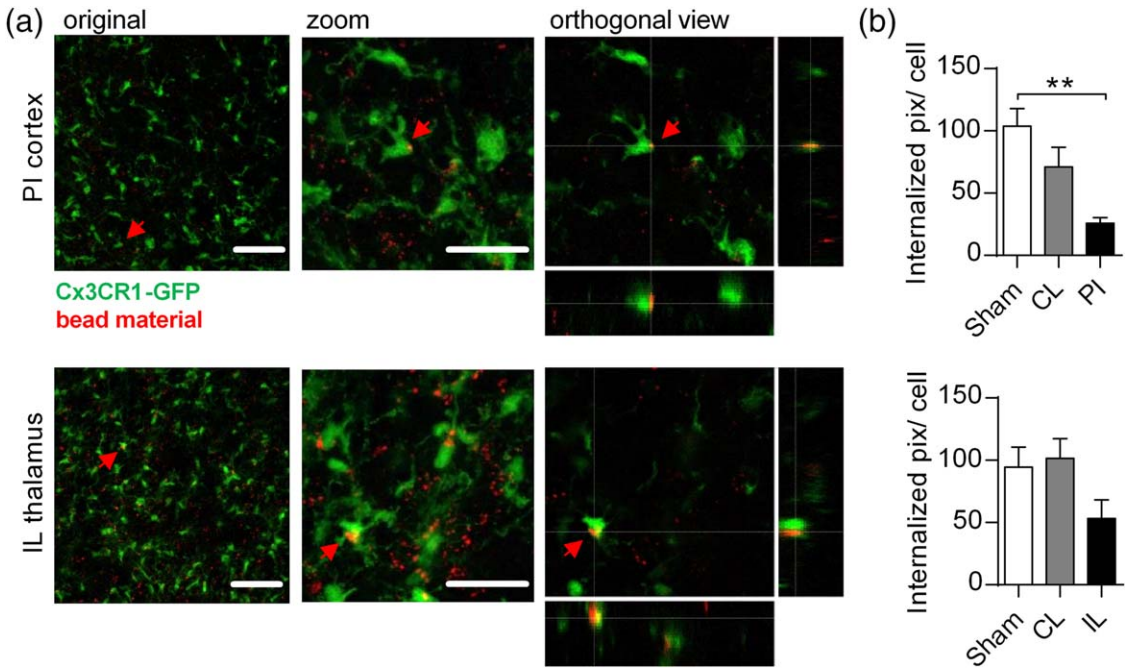

FIGURE 9 Microglia phagocytosis is reduced in the PI area but not the thalamus. (a) Representative confocal images of the PI and the ipsilateral thalamus 14 days after occlusion. Left panel indicates original images used for quantification. To determine internalization of bead material (red) higher magnification images were taken (middle panel) and visualized in orthogonal view (right panel). Engulfment of red bead material by green microglia is indicated by a red arrow. Scale bars, 25 μm. (b) Quantification of microglia phagocytosis in cortical and thalamic areas 14 days after stroke and in sham operated animals ($n = 5$, sham cortex; $n = 4$ stroke). $^{**}p < .01$ (one-way ANOVA followed by Tukey's multiple comparisons) [Color figure can be viewed at wileyonlinelibrary.com]

therefore evaluated the level of soluble Aβ oligomers instead. This is an important point of difference and the diseases processes under investigation are therefore not directly comparable. Interestingly, and in contrast to our own observations, Krabbe et al. also observed a reduction of phagocytic capacity (Figure 9; Krabbe et al., 2013).

In this study, the clearest molecular difference between the injury-responsive and non-responsive sites was the expression and cellular distribution of the P_2Y_{12} receptor. This receptor is responsible for the rapid process response to injury via binding of ATP released from damaged cells (Davalos et al., 2005; Haynes et al., 2006; Inoue, 2002). We identified, as has been previously reported, a reduction in the total level of P_2Y_{12} in the PI territories (Figure 5a,c) (Gelosa et al., 2014). In contrast, thalamic P_2Y_{12} receptor levels did not differ in terms of total protein levels but rather clustered strongly on the cell soma of non-responsive microglia within the thalamus (Figure 7d,f,h). No such somal clustering but rather a reduction in global expression was identifiable in the PI territories where microglia had retained their injury responsiveness (Figure 7c,e,g). Interestingly, microglia within the ipsilateral thalamus also failed to extend their processes towards locally applied ATP, the main ligand of the P_2Y_{12} receptor and signaling molecule directing process extension (Figure 6). Taken together, it seems likely that the high somal P_2Y_{12} receptor localization to the cell soma is related to the cells ability to respond to laser damage.

Given the rising evidence that P_2Y_{12} dependent purinergic signaling is involved in a multitude of microglia functions other than chemotaxis, maintaining P_2Y_{12} expression on the soma of non-responsive microglia might be required for functions other than process extension towards damage (Gu et al., 2016; Sipe et al., 2016; Swiatkowski et al., 2016). We therefore suggest that the spatial distribution of P_2Y_{12} rather than absolute protein levels is a potential factor in regulating microglia process migration and function.

In conclusion, this study demonstrates that the thalamus, a major site for stroke-induced SND, contains microglia that have lost the ability to respond to laser-induced damage. It is possible that this might be contributing to the progression of SND post-stroke. Alternatively, the loss of one function may promote other microglia functions targeted at containing neuronal degeneration. Given that a similar loss of process response has been described previously in other neurodegenerative disease models, we suggest that the here described microglia paralysis might be a more general microglia feature.

(f and g) Quantification of P_2Y_{12} process to soma immunoreactivity ratio for cortical (g) and thalamic regions (h) after stroke and in sham animals, respectively. Multilevel thresholding of the GFP fluorescent intensity was used to distinguish soma from process areas (left panels). The second channel for P_2Y_{12} immunoreactive signal was then overlaid and the intensity for each region, soma (middle panel) and processes (right panel), was assessed. ($n = 3$ images per animal; $n = 4$ animals per group). $^{*}p < .05$, $^{**}p < .01$, $^{***}p < .001$ (one-way ANOVA followed by Tukey's multiple comparisons).

ACKNOWLEDGMENT

The authors disclosed receipt of the following financial support for the research, authorship, and/or publication of this article. This study was

supported by the National Health and Medical Research Council (NHMRC) of Australia, Hunter Medical Research Institute, Faculty of Health and Medicine Pilot Grant and The University of Newcastle, Australia. F.R.W. and M.N. also acknowledge ongoing support from NHMRC Centre for Research Excellence in Stroke Recovery and Rehabilitation.

ORCID

Murielle G. Kluge http://orcid.org/0000-0002-9400-9094

REFERENCES

Block, F., Dihne, M., & Loos, M. (2005). Inflammation in areas of remote changes following focal brain lesion. *Progress in Neurobiology*, *75*, 342–365.

Chen, Y., Garcia, G. E., Huang, W., & Constantini, S. (2014). The involvement of secondary neuronal damage in the development of neuropsychiatric disorders following brain insults. *Frontiers in Neurology*, *5*, 22.

Dang, G., Chen, X., Chen, Y., Zhao, Y., Ouyang, F., & Zeng, J. (2016). Dynamic secondary degeneration in the spinal cord and ventral root after a focal cerebral infarction among hypertensive rats. *Scientific Reports*, *6*, 22655.

Davalos, D., Grutzendler, J., Yang, G., Kim, J. V., Zuo, Y., Jung, S., … Gan, W. B. (2005). ATP mediates rapid microglial response to local brain injury in vivo. *Nature Neuroscience*, *8*, 752–758.

Deschenes, M., Veinante, P., & Zhang, Z. W. (1998). The organization of corticothalamic projections: Reciprocity versus parity. *Brain Research. Brain Research Reviews*, *28*, 286–308.

Dirnagl, U., Iadecola, C., & Moskowitz, M. A. (1999). Pathobiology of ischaemic stroke: An integrated view. *Trends in Neurosciences*, *22*, 91–397.

Dissing-Olesen, L., LeDue, J. M., Rungta, R. L., Hefendehl, J. K., Choi, H. B., & MacVicar, B. A. (2014). Activation of neuronal NMDA receptors triggers transient ATP-mediated microglial process outgrowth. *Journal of Neuroscience*, *34*, 10511–10527.

Eyo, U. B., Gu, N., De, S., Dong, H., Richardson, J. R., & Wu, L. J. (2015). Modulation of microglial process convergence toward neuronal dendrites by extracellular calcium. *Journal of Neuroscience*, *35*, 2417–2422.

Fernandez-Andujar, M., Doornink, F., Dacosta-Aguayo, R., Soriano-Raya, J. J., Miralbell, J., Bargallo, N., … Mataro, M. (2014). Remote thalamic microstructural abnormalities related to cognitive function in ischemic stroke patients. *Neuropsychology*, *28*, 984–996.

Fetler, L., & Amigorena, S. (2005). Neuroscience. Brain under surveillance: The microglia patrol. *Science*, *309*, 392–393.

Gelosa, P., Lecca, D., Fumagalli, M., Wypych, D., Pignieri, A., Cimino, M., … Sironi, L. (2014). Microglia is a key player in the reduction of stroke damage promoted by the new antithrombotic agent ticagrelor. *Journal of Cerebral Blood Flow and Metabolism*, *34*, 979–988.

Gu, N., Eyo, U. B., Murugan, M., Peng, J., Matta, S., Dong, H., & Wu, L. J. (2016). Microglial P2Y12 receptors regulate microglial activation and surveillance during neuropathic pain. *Brain, Behavior, and Immunity*, *55*, 82–92.

Gyoneva, S., Swanger, S. A., Zhang, J., Weinshenker, D., & Traynelis, S. F. (2016). Altered motility of plaque-associated microglia in a model of Alzheimer's disease. *Neuroscience*, *330*, 410–420.

Haynes, S. E., Hollopeter, G., Yang, G., Kurpius, D., Dailey, M. E., Gan, W. B., & Julius, D. (2006). The P2Y12 receptor regulates microglial activation by extracellular nucleotides. *Nature Neuroscience*, *9*, 1512–1519.

Hines, D. J., Hines, R. M., Mulligan, S. J., & Macvicar, B. A. (2009). Microglia processes block the spread of damage in the brain and require functional chloride channels. *Glia*, *57*, 1610–1618.

Honda, S., Sasaki, Y., Ohsawa, K., Imai, Y., Nakamura, Y., Inoue, K., & Kohsaka, S. (2001). Extracellular ATP or ADP induce chemotaxis of cultured microglia through Gi/o-coupled P2Y receptors. *Journal of Neuroscience*, *21*,1975–1982.

Hooks, B. M., Mao, T., Gutnisky, D. A., Yamawaki, N., Svoboda, K., & Shepherd, G. M. (2013). Organization of cortical and thalamic input to pyramidal neurons in mouse motor cortex. *Journal of Neuroscience*, *33*, 748–760.

Inoue, K. (2002). Microglial activation by purines and pyrimidines. *Glia*, *40*, 156–163.

Jones, K. A., Zouikr, I., Patience, M., Clarkson, A. N., Isgaard, J., Johnson, S. J., … Walker, F. R. (2015). Chronic stress exacerbates neuronal loss associated with secondary neurodegeneration and suppresses microglial-like cells following focal motor cortex ischemia in the mouse. *Brain, Behavior, and Immunity*, *48*, 57–67.

Krabbe, G., Halle, A., Matyash, V., Rinnenthal, J. L., Eom, G. D., Bernhardt, U., … Heppner, F. L. (2013). Functional impairment of microglia coincides with Beta-amyloid deposition in mice with Alzheimer-like pathology. *PLoS One*, *8*, e60921.

Krishnamurthi, R. V., Feigin, V. L., Forouzanfar, M. H., Mensah, G. A., Connor, M., Bennett, D. A., … Murray, C.; Global Burden of Diseases, Injuries, Risk Factors Study 2010 (GBD 2010); GBD Stroke Experts Group. (2013). Global and regional burden of first-ever ischaemic and haemorrhagic stroke during 1990–2010: Findings from the Global Burden of Disease Study 2010. *The Lancet. Global Health*, *1*, e259–281.

Lalancette-Hebert, M., Gowing, G., Simard, A., Weng, Y. C., & Kriz, J. (2007). Selective ablation of proliferating microglial cells exacerbates ischemic injury in the brain. *Journal of Neuroscience*, *27*, 2596–2605.

Mahmoud Abdolhoseini, F. R. W., & Johnson, S. J. (2016). *Automated tracing of microglia using multilevel thresholding and minimum spanning trees*. Paper presented at the 38th International Conference of IEEE Engineering in Medicine and Biology Society (EMBC). Lake Buena Vista (Orlando), Florida, USA.

Mathiasen, M. L., Dillingham, C. M., Kinnavane, L., Powell, A. L., & Aggleton, J. P. (2017). Asymmetric cross-hemispheric connections link the rat anterior thalamic nuclei with the cortex and hippocampal formation. *Neuroscience*, *349*, 128–143.

Nimmerjahn, A., Kirchhoff, F., & Helmchen, F. (2005). Resting microglial cells are highly dynamic surveillants of brain parenchyma in vivo. *Science*, *308*, 1314–1318.

Ohsawa, K., Irino, Y., Sanagi, T., Nakamura, Y., Suzuki, E., Inoue, K., & Kohsaka, S. (2010). P2Y12 receptor-mediated integrin-beta1 activation regulates microglial process extension induced by ATP. *Glia*, *58*, 790–801.

Ohsawa, K., & Kohsaka, S. (2011). Dynamic motility of microglia: Purinergic modulation of microglial movement in the normal and pathological brain. *Glia*, *59*,1793–1799.

Ong, L. K., Guan, L., Damanhuri, H., Goodchild, A. K., Bobrovskaya, L., Dickson, P. W., & Dunkley, P. R. (2014). Neurobiological consequences of acute footshock stress: Effects on tyrosine hydroxylase phosphorylation and activation in the rat brain and adrenal medulla. *Journal of Neurochemistry*, *128*, 547–560.

Ong, L. K., Zhao, Z., Kluge, M., Walker, F. R., & Nilsson, M. (2016). Chronic stress exposure following photothrombotic stroke is associated with increased levels of Amyloid beta accumulation and altered oligomerisation at sites of thalamic secondary neurodegeneration in mice. *J Cereb Blood Flow Metab*. doi:10.1177/0271678X16654920

Orr, A. G., Orr, A. L., Li, X. J., Gross, R. E., & Traynelis, S. F. (2009). Adenosine A(2A) receptor mediates microglial process retraction. *Nature Neuroscience*, *12*, 872–878.

Patience, M. J., Zouikr, I., Jones, K., Clarkson, A. N., Isgaard, J., Johnson, S. J., … Nilsson, M. (2015). Photothrombotic stroke induces persistent ipsilateral and contralateral astrogliosis in key cognitive control nuclei. *Neurochemical Research*, *40*, 362–371.

Paxinos, G., & Franklin, K. (2001). *The Mouse Brain in Stereotaxic Coordinates*. San Diego, California: Elsevier.

Paz, J. T., Christian, C. A., Parada, I., Prince, D. A., & Huguenard, J. R. (2010). Focal cortical infarcts alter intrinsic excitability and synaptic excitation in the reticular thalamic nucleus. *Journal of Neuroscience*, *30*, 5465–5479.

Sasaki, Y., Hoshi, M., Akazawa, C., Nakamura, Y., Tsuzuki, H., Inoue, K., & Kohsaka, S. (2003). Selective expression of Gi/o-coupled ATP receptor P2Y12 in microglia in rat brain. *Glia*, *44*, 242–250.

Schafer, D. P., Lehrman, E. K., & Stevens, B. (2013). The "quad-partite" synapse: microglia-synapse interactions in the developing and mature CNS. *Glia*, *61*, 24–36.

Sieger, D., Moritz, C., Ziegenhals, T., Prykhozhij, S., & Peri, F. (2012). Long-range Ca2+ waves transmit brain-damage signals to microglia. *Developmental Cell*, *22*, 1138–1148.

Sipe, G. O., Lowery, R. L., Tremblay, M. E., Kelly, E. A., Lamantia, C. E., & Majewska, A. K. (2016). Microglial P2Y12 is necessary for synaptic plasticity in mouse visual cortex. *Nature Communications*, *7*, 10905.

Swiatkowski, P., Murugan, M., Eyo, U. B., Wang, Y., Rangaraju, S., Oh, S. B., & Wu, L. J. (2016). Activation of microglial P2Y12 receptor is required for outward potassium currents in response to neuronal injury. *Neuroscience*, *318*, 22–33.

Szalay, G., Martinecz, B., Lenart, N., Kornyei, Z., Orsolits, B., Judak, L., … Denes, A. (2016). Microglia protect against brain injury and their selective elimination dysregulates neuronal network activity after stroke. *Nature Communications*, *7*, 11499.

Tremblay, M. E., Lowery, R. L., & Majewska, A. K. (2010). Microglial interactions with synapses are modulated by visual experience. *PLoS Biology*, *8*, e1000527.

Tremblay, M. E., & Majewska, A. K. (2011). A role for microglia in synaptic plasticity? *Communicative & Integrative Biology*, *4*, 220–222.

Tynan, R. J., Beynon, S. B., Hinwood, M., Johnson, S. J., Nilsson, M., Woods, J. J., & Walker, F. R. (2013). Chronic stress-induced disruption of the astrocyte network is driven by structural atrophy and not loss of astrocytes. *Acta Neuropathologica*, *126*, 75–91.

van Groen, T., Puurunen, K., Maki, H. M., Sivenius, J., & Jolkkonen, J. (2005). Transformation of diffuse beta-amyloid precursor protein and beta-amyloid deposits to plaques in the thalamus after transient occlusion of the middle cerebral artery in rats. *Stroke*, *36*, 1551–1556.

Wake, H., Moorhouse, A. J., Jinno, S., Kohsaka, S., & Nabekura, J. (2009). Resting microglia directly monitor the functional state of synapses in vivo and determine the fate of ischemic terminals. *Journal of Neuroscience*, *29*, 3974–3980.

Wake, H., Moorhouse, A. J., & Nabekura, J. (2011). Functions of microglia in the central nervous system–beyond the immune response. *Neuron Glia Biology*, *7*, 47–53.

Walker, F. R., Beynon, S. B., Jones, K. A., Zhao, Z., Kongsui, R., Cairns, M., & Nilsson, M. (2014). Dynamic structural remodelling of microglia in health and disease: A review of the models, the signals and the mechanisms. *Brain, Behavior, and Immunity*, *37*, 1–14.

Zhang, J., Zhang, Y., Xing, S., Liang, Z., & Zeng, J. (2012). Secondary neurodegeneration in remote regions after focal cerebral infarction: A new target for stroke management? *Stroke*, *43*, 1700–1705.

SUPPORTING INFORMATION

Additional Supporting Information may be found online in the supporting information tab for this article.

How to cite this article: Kluge MG, Kracht L, Abdolhoseini M, et al. Impaired microglia process dynamics post-stroke are specific to sites of secondary neurodegeneration. *Glia*. 2017;65:1885–1899. https://doi.org/10.1002/glia.23201